

ChemComm

Chemical Communications

Accepted Manuscript

This article can be cited before page numbers have been issued, to do this please use: A. Avdoshin, W. Wenzel and M. Kozłowska, *Chem. Commun.*, 2025, DOI: 10.1039/D5CC01329A.



This is an Accepted Manuscript, which has been through the Royal Society of Chemistry peer review process and has been accepted for publication.

Accepted Manuscripts are published online shortly after acceptance, before technical editing, formatting and proof reading. Using this free service, authors can make their results available to the community, in citable form, before we publish the edited article. We will replace this Accepted Manuscript with the edited and formatted Advance Article as soon as it is available.

You can find more information about Accepted Manuscripts in the [Information for Authors](#).

Please note that technical editing may introduce minor changes to the text and/or graphics, which may alter content. The journal's standard [Terms & Conditions](#) and the [Ethical guidelines](#) still apply. In no event shall the Royal Society of Chemistry be held responsible for any errors or omissions in this Accepted Manuscript or any consequences arising from the use of any information it contains.

Journal Name

ARTICLE TYPE

Cite this: DOI: 00.0000/xxxxxxxxxx

Confinement-modulated diffusion of alkenes in NU-1000 framework material[†]Aleksandr Avdoshin,^a Wolfgang Wenzel,^a and Mariana Kozłowska^{*a}

Received Date

Accepted Date

DOI: 00.0000/xxxxxxxxxx

Metal-organic frameworks (MOFs) and similar molecular frameworks are increasingly investigated in catalysis for energy applications due to the tunability of these materials for spatially controlled positioning of catalytic active sites, combined with tailor-made porosity. However, because of the complex interplay of catalytic reactions and diffusion processes, the influence of the framework is not well understood. In this study, we used molecular dynamics (MD) and grand canonical Monte Carlo (GCMC) simulations to explore the confinement effects of the NU-1000 MOF on the diffusivity and adsorption of α -olefins. We provide a direct comparison of diffusion coefficients under non-confined conditions and a reduction in diffusion constants primarily governed by MOF-olefin interactions rather than olefin-olefin interactions, with higher mobility along the channel axis than perpendicular to it.

MOFs are promising carrier materials for single atom catalysts (SAC)^{1–3} due to their tunable composition⁴, structural stability⁴, SAC stabilization at the atomistic level⁵, and ease of product separation⁶. They are beneficial especially for reactions demonstrating the crucial role of selectivity, e.g. ethylene oligomerization. For example, Ni-grafted MOFs demonstrated activity levels, raising ethylene conversion, that are one to two orders of magnitude higher than classical porous materials like zeolites and oxides⁷. The elevated activity is influenced by confinement effects and the coordination of metals⁸. Similar observations were reported for NU-1000 MOF⁹ (schematically shown in Figure 1A, B) after its functionalization with SAC^{10,11}. This MOF features a hierarchical pore structure with mesochannels and microchannels, enabling selective reagent adsorption and diffusion, making it well-suited for catalysis and ethylene oligomerization^{10–12}, previously studied in NU-1000 at ~300 K and 1–15 bar^{10,12}. Note that common conditions reported for porous materials span wider ranges, for example 300–600 K and 1–50 bar¹³.

While metal catalysts exploit local electronic properties, MOF confinement additionally governs selectivity, kinetics, and separation via diffusion and adsorption. Haag¹⁴ showed cracking chain-length effects stem from stronger adsorption of longer hydrocarbons in zeolites rather than variations in zeolite acidity. Bickel and Gounder¹⁵ reported the change in catalytic performances by the dynamic composition of in-pore species and additional diffusional constraints on reactants and products during chain-growth reactions in porous catalysts. However, detailed investigations of these effects remain scarce: recent reviews note that studies beyond binary mixtures are rare and overwhelmingly centered on alkanes^{16,17}.

Here, we employ GCMC/MD simulations to investigate the co-adsorption and diffusion of a full homologous series of α -olefins (C₂–C₁₀) within the hierarchical pores of NU-1000, considering typical experimental conditions used for ethylene oligomerization. Due to its proven thermophysical and vapor-liquid equilibrium accuracy^{18,19}, we perform simulations by combining the Extension of the Universal Force Field for Metal–Organic Frameworks (UFF4MOF) for unmodified NU-1000 MOF and Transferable Potentials for Phase Equilibria (TraPPE) force field for guest molecules (see Supplementary Information (SI) for more details).

For NU-1000, like other mesoporous materials, type IV or V isotherms are typical according to the International Union of Pure and Applied Chemistry classification²⁰. NU-1000 shows type IV isotherms for N₂²¹, indicating weak adsorbate–adsorbent interactions²⁰. For the adsorption of C₄H₈ and C₆H₁₂ in NU-1000, we observe a type I isotherm (Figure 1C), which is typically associated with microporous materials and strong adsorbate–adsorbent interactions. This behavior arises from significantly stronger van der Waals interactions of olefins with the MOF scaffold^{22,23} and the contribution of microchannels of NU-1000, as we discuss further. A similar type I-like isotherm profile was reported for n-butane in NU-1000 at pressure below saturation²⁴, and for 1-butene in MOF-74²⁵. Heavier olefins in the liquid phase (Figure 1E), as well as C₄H₈ at $P > P_o$, exhibit negligible pressure dependence, indicating pore saturation.

^a Institute of Nanotechnology, Karlsruhe Institute of Technology, Kaiserstr. 12, 76131 Karlsruhe, Germany. E-mail: mariana.kozłowska@kit.edu

[†] Supplementary Information available: [details of any supplementary information available should be included here]. See DOI: 00.0000/00000000.



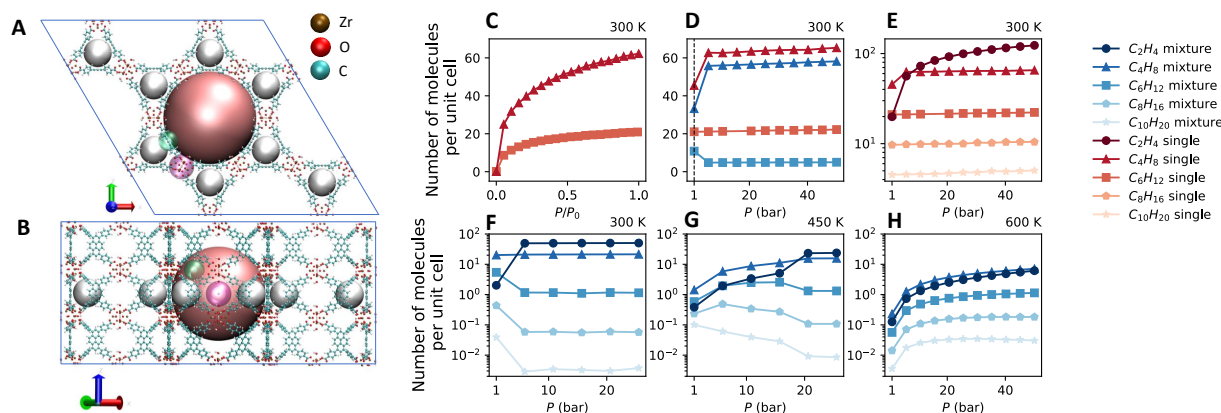


Fig. 1 Visualization of $2 \times 2 \times 2$ unit cell of NU-1000: (A) Viewed along the z-direction (blue arrow) and (B) Viewed along the in x-y-plane (red and green arrows). Hexagonal mesochannels of 32 Å, (pink spheres) triangle microchannels of 12 Å (white spheres), windows between mesochannels of 8 Å (purple transparent sphere), and a microchannel and mesochannel (green transparent sphere) with the size of 7 Å are marked for clarity. GCMC-simulated adsorption isotherms of olefins: (C) For single-component C_4H_8 (saturation pressure $P_0 = 3.14$ bar) and C_6H_{12} ($P_0 = 0.27$ bar) at 300 K. (D) Comparison of single-component and equimolar systems of two components C_4H_8 and C_6H_{12} at 300 K. (E) Single component systems C_2H_4 – $C_{10}H_{20}$ at 300K. (F) – (H) Equimolar systems of five components olefins ranging from C_2H_4 to $C_{10}H_{20}$ at 300 K, 450 K, and 600 K, respectively.

In olefin mixtures, the mutual influence of other molecules is evident, for example, when comparing the adsorption of C_4H_8 and C_6H_{12} independently (i.e. as single components) versus their equimolar mixture (Figure 1D). While C_6H_{12} alone shows negligible pressure dependence, in the presence of C_4H_8 , its adsorption typically decreases with increasing pressure from 5 to 10 bars. This behavior stems from competitive adsorption, where increased C_4H_8 uptake at high pressures displaces C_6H_{12} . Such mutual influence is also observed in equimolar mixtures of more than two olefins, as shown in Figure 1F. Lighter components (C_2H_4 to C_4H_8) replace heavier olefins in NU-1000 until the plateau corresponding to saturation is reached. While lighter olefins exhibit a monotonic increase in adsorption, heavier ones, such as $C_{10}H_{20}$, show a monotonic decrease. Olefins with saturation pressures within this range (see Section 5 in SI), such as C_6H_{12} , display non-monotonic behavior, increasing until $P = 15.7$ bar before decreasing as the phase transitions occur (Figure 1G). As the temperature elevates, more olefins exhibit a monotonic behavior with their loading increasing consistently with the pressure increase (see Figure 1H). In addition, typically, the adsorption capacity diminishes with the chain length increase, i.e. as observed for olefins ranging from C_4H_8 to $C_{10}H_{20}$. However, in the case of C_2H_4 , the adsorption capacity is lower than that of C_4H_8 . In the provided examples (Figure 1F, G), within the pressure range of 25 to 50 bars, there is no substantial variation in the adsorption behavior (see Figure S5).

To elucidate the adsorption sites of olefins in NU-1000, we analyzed the spatial distribution of molecules from GCMC simulations at 300 K using C_4H_8 as an example, an olefin with the highest adsorption loading (see Figure 2A). It can be seen that the molecules are more evenly distributed throughout the triangle microchannels, while adsorption in the hexagonal mesochannel occurs primarily near the MOF linkers rather than in the channel center or near the metal node in mesochannel. A similar tendency was reported in the binding energies and adsorption en-

thalpies from the density functional theory calculations of CH_4 and C_2H_6 in NU-1000, showing a preference for microchannel corners over metal nodes²², and for pore edges over the pore center²⁶. Moreover, olefins may interact with the pyrene-based linkers in NU-1000 via π -based interactions²⁷, explaining adsorbate distribution near the aromatic rings. There is a probability for C_4H_8 adsorption directly on the metal node within the microchannel; however, a different perspective (Figure S6A) reveals that olefins are actually concentrated in the windows between the mesochannels. This behavior can be linked to the common placement of catalytic sites in NU-1000 nodes in windows between mesochannels (see Figure S7).

To quantify the probability of the fractional occupancy of olefins within different channels, the free energy difference for moving of olefin's carbon atoms from a micro to mesochannel was calculated using the equation: $\Delta G = -k_B T \ln \frac{\rho_{meso}}{\rho_{micro}}$, where ρ_{micro} and ρ_{meso} denote the probabilities of an olefin's carbon atoms being in a microchannel or mesochannel. These probabilities were calculated from GCMC snapshots (see section 3 in SI). In Figure 2B, values below zero (the dashed line) indicate a preference for adsorption in mesochannel, whereas values above the dashed line indicate a preference for adsorption in microchannel. The results show that single-component C_2H_4 at 1 bar prefers to occupy the microchannel. As pressure increases, enhanced ethylene adsorption saturates the microchannel, shifting olefin uptake to the mesochannel regions. It is consistent with the observation of microchannels saturation reported by Vergas L.²⁴. For C_4H_8 , mesochannel adsorption is already favored at 1 bar, with this preference becoming even stronger as pressure rises. For heavier olefins (C_6H_{12} – C_8H_{16}) in single component systems, the distribution of their fractional occupancy remains consistent across the pressure range as adsorption loading remains constant, indicating a strong preference for microchannel.

In mixed-component systems, the distribution of fractional occupancies of reagents across different channel types is mutually



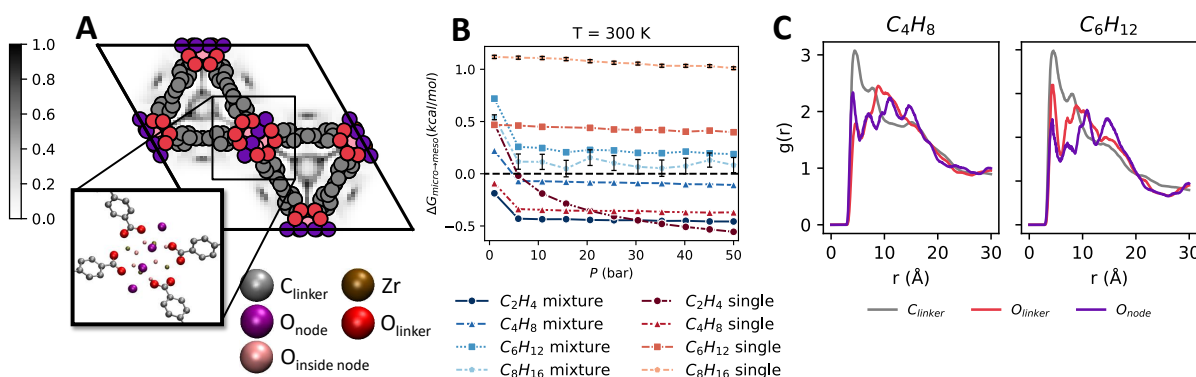


Fig. 2 (A) Heat map displaying the normalized probability distribution of C_4H_8 adsorption in NU-1000 MOF in z-direction; darker regions indicate higher probability of finding a molecule at specific position. (B) The free energy change associated with transferring an olefin's carbon atoms from a triangle microchannel to a hexagonal mesochannel as a function of loading corresponding to specific pressure. The statistical uncertainty of ΔG is given in Figure S4. (C) The radial distribution function (RDF) of distances between the olefin and the framework considering different atomic sites.

influenced. Compared to single-component systems, atoms of C_4H_8 tend to shift toward the microchannels, thereby displacing other species into the mesochannels. This effect is evident in Figure 2B, where the single-component curves generally lie above their corresponding blue curves, except for C_4H_8 . This trend is even clearer when contrasted with coadsorption scenarios lacking C_4H_8 (see Figure S9). Across all pressures, fractional occupancies of olefins exhibit a greater $\Delta G_{micro \rightarrow meso}$ compared to those olefins that include C_4H_8 . A similar, though less pronounced, behavior is observed for C_2H_4 at pressures above 30 bar and for C_6H_{12} at 1 bar. Furthermore, microchannel saturation is observed for all olefins at pressures between 1 and 5 bar.

To further investigate the microscopic differences in olefin interactions near the metal nodes, we analyzed the RDF of the selected atomic distances between adsorbates single system component C_4H_8 and C_6H_{12} and a MOF using MD simulations that incorporate GCMC loading data at $T = 300$ K under various pressures. Since the differences of RDF across loadings were negligible, the results at $P = 50$ bar are demonstrated in Figure 2C (see more details in SI). The RDF analysis identified three primary adsorption sites in NU-1000: the carbon and oxygen atoms of the linkers, and the oxygen atom of the metal node (see Figure 2A,C). For olefin adsorption site, the terminal sp^2 carbon of the α -olefin double bond was selected for the RDF analysis due to its role in the olefin oligomerization reactions.

From the analysis of the distances between atoms of the adsorbate and the MOF, the most favorable adsorption site for C_4H_8 and C_6H_{12} was found near carbon atoms of the linker (in gray in Figure 2C) at a distance of 4.4 Å. It complements the result of the normalized probability distribution of olefin adsorption obtained in GCMC (Figure 2A and S6 in SI). For C_4H_8 , the RDF reveals a second peak corresponding to the metal node oxygen at 4.1 Å with a peak height of 2.3, indicating a close interaction between the olefin and the node oxygen. In contrast, the peak associated with the linker oxygen atom is observed at 4.6 Å with a lower height of 1.8. However, for C_6H_{12} , the peak, indicating the close contact between adsorbates and the oxygen atom from

the linker, dominates over the oxygen of the metal node with a closer distance at 4.3 Å and an RDF peak height of 3.2, while the peak at the node oxygen has a lower height of 2.4. In general, shorter distances between C_6H_{12} and the oxygen atoms are more populated than with C_4H_8 . We attribute the closer peak positions for node oxygen to the large hexagonal channel topology, which features a wide 120° opening that provides ample space for olefins to interact with the metal nodes. Similarly, olefins located in the windows between mesochannels benefit from this wide opening, facilitating their interaction with the metal nodes. Moreover, the higher peaks observed for C_6H_{12} near the oxygen atoms of the linkers are attributed to a stronger preference of the microchannels for C_6H_{12} in single-component systems compared to C_4H_8 (see Figure 2B). Lighter olefins exhibit lower peak intensities across all atomic sites (see Figure S8 in SI), indicating higher mobility. This enhanced mobility is advantageous, as ethylene plays a critical role in the oligomerization process.

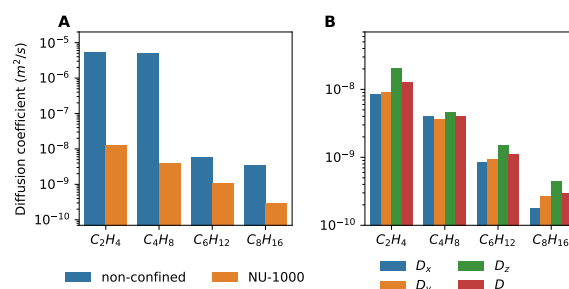


Fig. 3 (A) Diffusion coefficients of olefins in non-confined and confined environments at 1 bar and 300 K. (B) Anisotropic diffusion of olefins in D_x , D_y , D_z directions and overall diffusion D .

Olefin mobility in the MOF can be estimated by the calculation of self-diffusion coefficients. To this end, we have computed the mean squared displacement (MSD) using 100 ns MD simulations at various loadings according to GCMC data (see SI for details). To assess the effect of MOF confinement on self-diffusion, we also calculated diffusion coefficients for non-confined systems (a box



containing pure olefin). Due to limitations in the MSD approach, which applies only to molecules with sufficiently fast diffusion, we report diffusion coefficients only for olefins up to C_8H_{16} in single component systems. They are depicted in Figure 3. Due to spatial restrictions in NU-1000, olefin diffusion coefficients drop by two orders of magnitude compared to non-confined conditions for C_2H_4 - C_4H_8 and one order for C_6H_{12} - C_8H_{16} . Unlike in non-confined systems, diffusion in NU-1000 decreases more gradually with chain length, highlighting their distinct confinement effects.

Due to NU-1000's anisotropic structure with one-dimensional channels aligned along the crystallographic axes anisotropic diffusion is expected (Figure 3 B). Our findings confirm this expectation: the diffusion coefficient along the channel axis, D_z , exceeds those in the perpendicular directions, D_x and D_y . For instance, C_2H_4 exhibits diffusion along D_z that is 2.4 times higher than in the perpendicular directions, while for C_4H_8 it is 1.2, for C_6H_{12} it is 1.7, and for C_8H_{16} it is 2. These results, obtained within loading boundaries, are in good agreement with Vargas *et al.*²⁴.

By explicitly accounting for multicomponent interactions, our findings demonstrate that the confinement effect of NU-1000 leads to a selective segregation of α -olefins, driven by their complex co-adsorption behavior, where lighter olefins displace heavier ones. Moreover, the unique topology of NU-1000 induces an internal separation: heavier olefins preferentially occupy the microchannels, while lighter ones are more abundant in the mesochannels. Our investigation suggests that positioning the catalytic sites on the metal nodes oriented toward the mesochannels is advantageous, as these sites benefit from the high accessibility afforded by the mesochannel topology. The confinement effect results in a significant decrease in diffusion coefficients and induces anisotropic diffusion compared to non-confined environments, thereby facilitating product separation. These insights are valuable for developing kinetic models that incorporate mass transfer limitations and product-specific concentration profiles.

Acknowledgements

This research was funded by the Deutsche Forschungsgemeinschaft (DFG) via GRK 2450.

Conflicts of interest

There are no conflicts to declare.

Data availability

Data generated is available within the NOMAD Repository <https://dx.doi.org/10.17172/NOMAD/2025.07.08-1>.

Notes and references

- Y.-S. Wei, M. Zhang, R. Zou and Q. Xu, *Chemical Reviews*, 2020, **120**, 12089–12174.
- A. Bavykina, N. Kolobov, I. S. Khan, J. A. Bau, A. Ramirez and J. Gascon, *Chemical Reviews*, 2020, **120**, 8468–8535.
- D. Yang and B. C. Gates, *ACS Catalysis*, 2019, **9**, 1779–1798.
- V. F. Yusuf, N. I. Malek and S. K. Kailasa, *ACS Omega*, 2022, **7**, 44507–44531.
- V. Mouarrawis, R. Plessius, J. I. van der Vlugt and J. N. H. Reek, *Frontiers in Chemistry*, 2018, **6**, 623.
- Y. Duan, L. Li, Z. Shen, J. Cheng and K. He, *Membranes*, 2023, **13**, 480.
- A. Peng, Z. Huang and G. Li, *Catalysts*, 2024, **14**, 268.
- R. Rajapaksha, P. Samanta, E. A. Quadrelli and J. Canivet, *Chemical Society Reviews*, 2023, **52**, 8059–8076.
- J. E. Mondloch, W. Bury, D. Fairen-Jimenez, S. Kwon, E. J. DeMarco, M. H. Weston, A. A. Sarjeant, S. T. Nguyen, P. C. Stair, R. Q. Snurr, O. K. Farha and J. T. Hupp, *Journal of the American Chemical Society*, 2013, **135**, 10294–10297.
- T. A. Goetjen, X. Zhang, J. Liu, J. T. Hupp and O. K. Farha, *ACS Sustainable Chemistry and Engineering*, 2019, **7**, 2553–2557.
- J. Ye, L. Gagliardi, C. J. Cramer and D. G. Truhlar, *Journal of Catalysis*, 2018, **360**, 160–167.
- S. T. Madrahimov, J. R. Gallagher, G. Zhang, Z. Meinhart, S. J. Garibay, M. Delferro, J. T. Miller, O. K. Farha, J. T. Hupp and S. T. Nguyen, *ACS Catalysis*, 2015, **5**, 6713–6718.
- A. Finiels, F. Fajula and V. Hulea, *Catal. Sci. Technol.*, 2014, **4**, 2412–2426.
- W. Haag, in *Catalysis by Zeolites – Science and Technology*, Elsevier, 1994, p. 1375–1394.
- E. E. Bickel and R. Gounder, *JACS Au*, 2022, **2**, 2585–2595.
- H. Daglar, H. C. Gulbalkan, G. O. Aksu and S. Keskin, *Advanced Materials*, 2024.
- H. Wang, D. Luo, E. Velasco, L. Yu and J. Li, *Journal of Materials Chemistry A*, 2021, **9**, 20874–20896.
- B. L. Eggimann, A. J. Sunnarborg, H. D. Stern, A. P. Bliss and J. I. Siepmann, *Molecular Simulation*, 2013, **40**, 101–105.
- U. of Minnesota, *Transport Phenomena*, <http://trappe.oit.umn.edu>, 2024, Accessed: 2024-08-29.
- M. Thommes, K. Kaneko, A. V. Neimark, J. P. Olivier, F. Rodriguez-Reinoso, J. Rouquerol and K. S. Sing, *Pure and Applied Chemistry*, 2015, **87**, 1051–1069.
- G. Mercuri, M. Moroni, S. Galli, G. Tuci, G. Giambastiani, T. Yan, D. Liu and A. Rossin, *ACS Applied Materials & Interfaces*, 2021, **13**, 58982–58993.
- W. Zhang, Y. Ma, I. A. Santos-López, J. M. Lownsbury, H. Yu, W.-G. Liu, D. G. Truhlar, C. T. Campbell and O. E. Vilches, *Journal of the American Chemical Society*, 2017, **140**, 328–338.
- G. O. Vissers, W. Zhang, O. E. Vilches, W.-G. Liu, H. S. Yu, D. G. Truhlar and C. T. Campbell, *The Journal of Physical Chemistry C*, 2019, **123**, 6586–6591.
- E. Vargas L. and R. Q. Snurr, *Langmuir*, 2015, **31**, 10056–10065.
- B. R. Barnett, S. T. Parker, M. V. Paley, M. I. Gonzalez, N. Biggins, J. Oktawiec and J. R. Long, *Journal of the American Chemical Society*, 2019, **141**, 18325–18333.
- A. E. Platero-Prats, A. Mavrandonakis, J. Liu, Z. Chen, Z. Chen, Z. Li, A. A. Yakovenko, L. C. Gallington, J. T. Hupp, O. K. Farha, C. J. Cramer and K. W. Chapman, *Journal of the American Chemical Society*, 2021, **143**, 20090–20094.
- R. Abazari, S. Sanati, M. A. Bajaber, M. S. Javed, P. C. Junk, A. K. Nanjundan, J. Qian and D. P. Dubal, *Small*, 2024, **20**, 2306353.



Confinement-modulated diffusion of alkenes in NU-1000 framework materialView Article Online
DOI: 10.1039/D5CC01329A

Aleksandr Avdoshin, Wolfgang Wenzel, and Mariana Kozłowska

Data availability statement**1. Data generated is available within the NOMAD Repository**<https://url.uk.m.mimecastprotect.com/s/cZepCE8VxfpRpNrSNf3s7E99g?domain=dx.doi.org>.